

ChemComm

Accepted Manuscript



This is an *Accepted Manuscript*, which has been through the Royal Society of Chemistry peer review process and has been accepted for publication.

Accepted Manuscripts are published online shortly after acceptance, before technical editing, formatting and proof reading. Using this free service, authors can make their results available to the community, in citable form, before we publish the edited article. We will replace this *Accepted Manuscript* with the edited and formatted *Advance Article* as soon as it is available.

You can find more information about *Accepted Manuscripts* in the [Information for Authors](#).

Please note that technical editing may introduce minor changes to the text and/or graphics, which may alter content. The journal's standard [Terms & Conditions](#) and the [Ethical guidelines](#) still apply. In no event shall the Royal Society of Chemistry be held responsible for any errors or omissions in this *Accepted Manuscript* or any consequences arising from the use of any information it contains.

Determination of the Magnetic Anisotropy in a Multinuclear Tb^{III}-Based Single-Molecule Magnet†

Cite this: *Chem. Commun.*, 2014, *?*, *?*

Received 00th January 2014,
Accepted 00th January 2014

Xing-Cai Huang,^a Veacheslav Vieru,^b Liviu F Chibotaru,^{*b} Wolfgang Wernsdorfer,^c Shang-Da Jiang^{*d} and Xin-Yi Wang^{*a}

DOI: 10.1039/x0xx00000x

www.rsc.org/chemcomm

Magneto-structural relationship was studied experimentally and theoretically for two enantiomeric tetranuclear [CuTb]₂ SMMs. For the first time, the determination of the magnetic anisotropy axis on an individual magnetic ion, the Tb³⁺, was achieved in a polynuclear Tb³⁺-based SMM.

Magnetic anisotropy provides directionality and stability to magnetization. It is the key ingredient to the coercive field and magnetic energy of bulk magnets,¹ and to the performance of the single-molecule magnets (SMMs),² which has invoked intense interest in the field of spintronic devices³ and quantum computing.⁴ However, magnetic anisotropy is also the most difficult to manipulate, especially for the lanthanides which dominated the current SMM researches.⁵ Theoretically, phenomenological crystal field models have been used for decades to explain the magnetic properties of lanthanides.⁶ A popular version of this approach is the electrostatic point charge model,⁷ in which the charges are taken either as phenomenological parameters^{7a-c} or extracted from DFT calculations.^{7d} Fast progress of quantum chemistry methods and increased computational power made it possible to use nowadays fully *ab initio* methods to describe the anisotropy of relatively large complexes.⁸ In combination with the intuitive understanding that axial (equatorial) ligand field favors the easy axis anisotropy of oblate (prolate) 4f electron distribution,⁹ these methods have permitted a full description of magnetic anisotropy in lanthanides.

Experimentally, the anisotropy measurements on a wide range of transition metal and lanthanide complexes has been reported and reviewed in the 1970s.¹⁰ Recently, the angular-resolved magnetometry measurement has been proved to be very useful for the magnetic anisotropy investigation on some lanthanide SMMs with one unique lanthanide center, including several Dy^{III}, Er^{III}, and Yb^{III} single-ion compounds.¹¹⁻¹³ For the Tb^{III}-compounds, the angular-resolved experiment was also performed on the Tb-DOTA complex, which is unfortunately not an SMM.^{11b} On the other hand, of all the lanthanide centers, the Tb³⁺ ion is of predominant importance. Although the Tb-SMMs are less numerous compared to the Dy-SMMs due to its non-Kramers nature,^{5a,9b} the Tb-SMMs accounted for some of the most impressive results, including the first and most widely studied Ln-SMM (double-decker terbium complex [TbPC₂]),¹⁴ the first 3d-4f SMM ([CuLTb(hfac)₂]),¹⁵ the SMM of the highest energy barrier ([TbPC₂],

$U_{\text{eff}} = 652 \text{ cm}^{-1} = 938 \text{ K}$),¹⁶ and the highest blocking temperature ($\{[(\text{Me}_3\text{Si})_2\text{N}]_2(\text{THF})\text{Tb}\}_2(\mu\text{-N}_2)$, $T_{\text{B}} = 14 \text{ K}$).¹⁷ Thus, knowledge on the anisotropy of the Tb^{III}-SMMs will be of great value for the design and construction of better SMMs.

Recently, we reported a tetranuclear [CuTb]₂-valpn SMM where the Tb³⁺ ions were bridged solely by the end-on azides.¹⁸ Direct experiment confirmation of the easy axis using the angular-resolved measurement was hindered by the small size of the single crystals. Herein, we report the detailed characterization and magnetic property determination of the Tb^{III} ion in two enantiomeric tetranuclear SMMs [Cu₂(valchxn)₂Tb₂(N₃)₆]-2CH₃OH (**1-RR** and **1-SS**, H₂valchxn (*R,R*)- and (*S,S*)-1,2-cyclohexanediylbis(2-iminomethylene-6-methoxy-phenol)). The magneto-structural relationship and the direction of the principal magnetic axis of this cluster have also been verified by detailed *ab initio* calculation.

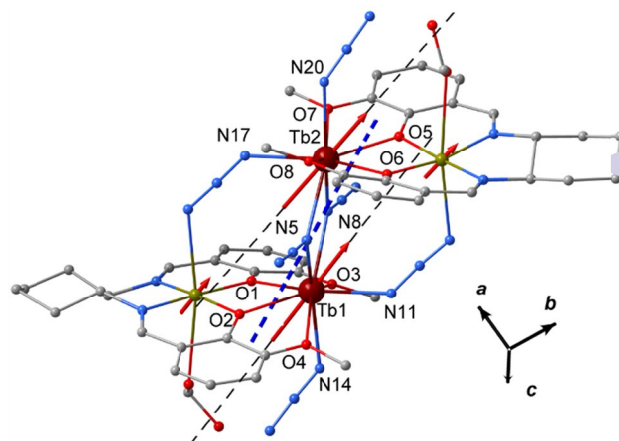


Fig. 1 The structure of **1-RR** showing the double EO azido-bridged [CuTb]₂ cluster. The blue dashed line represents the easy axis from the experiment, and the red ones are the *ab initio* calculated orientations of the local magnetic moments in the ground exchange doublet.

The structures of **1-RR** and **1-SS** were very similar to the reported [CuTb]₂-valpn compound (Fig. 1). Several points are worth mentioning. 1) They crystallized in the triclinic space group P1 with only one [CuTb]₂ cluster in the unit cell; 2) The two phenolic oxygen-bridged [CuTb] units were related to each other by a pseudo-inversion center and bridged by two EO azide; and 3) The Tb³⁺ ions are in the

bicapped trigonal prism environment with very long Tb-O bonds for the capping atoms (O₃, O₄, O₇, and O₈). These methoxy oxygen atoms bear much less negative charges compared to the deprotonated phenolic oxygen atoms and the nitrogen atoms of azides, leading to an axial negative charge distribution around the Tb³⁺ centers.

Compounds **1-RR** and **1-SS** show the same magnetic properties with negligible differences (ESI for details), and we will only discuss the properties of **1-RR** in details. Upon cooling, the $\chi_m T$ curve (Fig. S4) decreases from the room temperature value 25.15 cm³mol⁻¹K to a minimum around 50 K, and increases again until 2 K, suggesting the dominant ferromagnetic interactions between the phenolic oxygen bridged Cu-Tb and the azide bridged Tb-Tb pairs, consistent with the theoretical analysis (vide post) and the reported results.^{15,28-29} The non-superposition of the M vs H/T data to a single master curve and the low magnetization of 11.3 μ_B at 7 T suggest the presence of a significant magnetic anisotropy (Fig. S5-6). Temperature and frequency dependences of the ac susceptibilities under a zero dc field (Fig. 2 and S7) reveal a slow relaxation of the magnetization. The analyses on the ac data using the generalized Debye model²⁰ (Table S3) and the Arrhenius law gave the following parameters: $\alpha \leq 0.17$, $U_{\text{eff}} = 27.6 \pm 0.2$ K (19.2 \pm 0.1 cm³), and $\tau_0 = (2.03 \pm 0.05) \times 10^{-5}$ s. Above 1.8 K, a thermally activated Orbach relaxation process with a narrow distribution of relaxation times was confirmed.

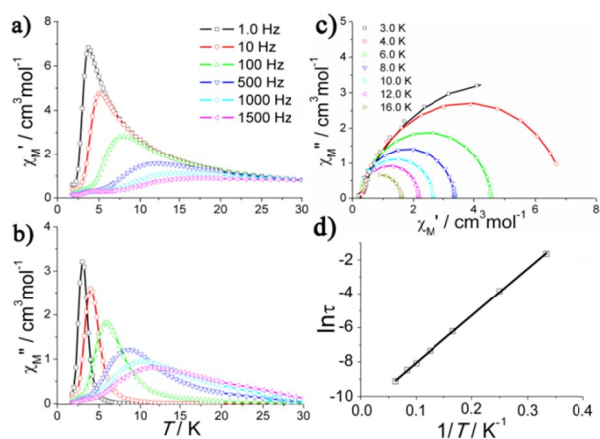


Fig. 2 (a-b) Temperature dependence of the ac susceptibilities for **1-RR** under $H_{\text{ac}} = 5$ Oe and $H_{\text{dc}} = 0$ Oe; (c) Cole-Cole plots for **1-RR**. The lines represent the fitting using the generalized Debye model; (d) the Arrhenius plot of **1-RR**.

The SMM behavior of **1-RR** was confirmed by the hysteresis loops measured on a field-oriented single crystal ($m = 0.93$ mg) on a conventional SQUID-VSM above 1.8 K (Fig. S13) and on a μ -SQUID down to 0.03 K (Fig. 3). At a field sweep rate of 0.14 T/s, magnetic hysteresis is observed at temperatures up to 4.0 K. Above 1.4 K, the coercivities increase with decreasing temperature as expected for SMMs, reaching 4.6 kOe at 1.4 K. Quantum tunnelling of the magnetization (QTM) is evidenced by the observation of temperature-independent loops below 1.4 K that remain strongly dependent on the field sweep rate. Step-like features were clearly observed for the loops. As can be seen from the dM/dH curves (Fig. S14-S15), the critical fields at higher field are proportional to the field sweep rates, while the critical field for the steps near zero field (0.8 kOe) is independent on the field sweep rate and the temperature, indicating that **1-RR** is an exchange-biased SMM.²²

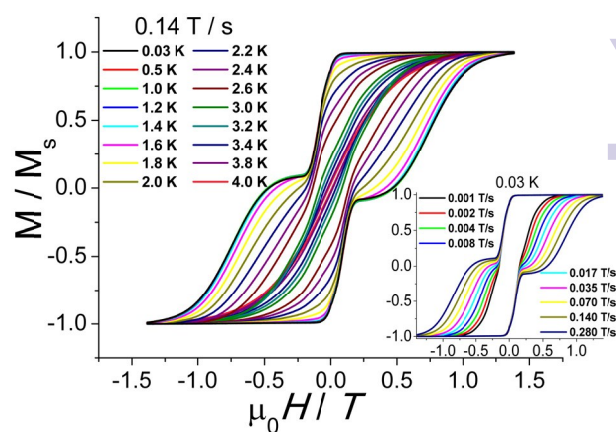


Fig. 3 The hysteresis loops of **1-RR** measured on a single crystal on a μ -SQUID at the indicated temperatures and field sweep rates.

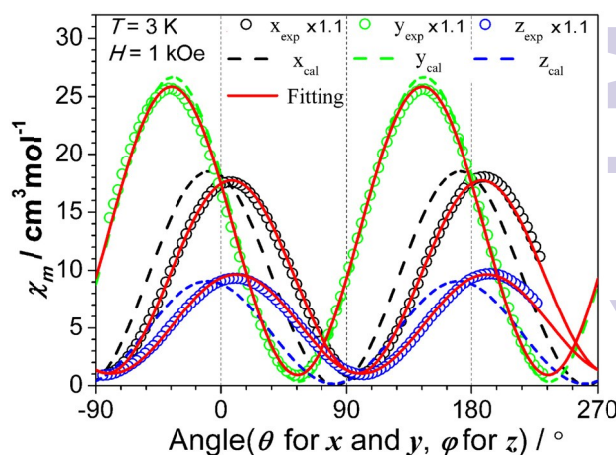


Fig. 4 Angular dependence of the magnetic susceptibility of **1-RR** at 3.0 K for the rotation along the three axes of the laboratory frame. The red solid lines and the dashed lines represent the fitted curves and the ones obtained from the *ab initio* calculation. The experiment curves were upscaled by 10%.

The Ising anisotropy of the cluster and the Tb³⁺ centers can be revealed by the angular resolved magnetometry measurement based on the following two criteria. 1) **1-RR** crystallizes in a triclinic space group with only one unique [CuTb]₂ unit in the unit cell, which guarantees the determination of the susceptibility tensor of the whole [CuTb]₂ unit.¹¹⁻¹³ 2) The Cu²⁺ ions contribute little to the molecular magnetic anisotropy and the two ferromagnetically coupled Tb centers are related by a pseudo-inversion center, which ensures the rough colinearity of the easy axis of each Tb³⁺ with that of the whole molecule. The angular dependence of the magnetic susceptibility was measured on a face-indexed single crystal ($m = 0.43$ mg, Fig. S16) mounted on a L-shaped Cu:Be support from 1.8 to 15 K (Fig. 4 and Fig. S17-19). Apparent strong magnetic anisotropy was observed at all temperatures. The positions of the maxima of the curves were found to shift considerably below 2.5 K. This phenomenon is most likely connected to the low-temperature magnetic hysteresis, which generates a non-equilibrium situation during the rotation.^{12a} The susceptibility tensors and their principal values were extracted by simultaneously fitting the angular dependence data to the three rotation functions and subsequent diagonalizing the susceptibility

tensors (solid lines in Fig. 4, Table S5). At 3 K, the largest principle value of the susceptibility tensor is $23.54 \text{ cm}^3\text{mol}^{-1}$ while the other two are close to $1 \text{ cm}^3\text{mol}^{-1}$, confirming the strong Ising anisotropy of the $[\text{CuTb}]_2$ cluster. This Ising anisotropy is evident at all temperatures, as can be seen from the big difference of the $\chi_M T$ vs T plots along different principle axes (Fig. S20). The obtained orientation of the molecular easy axis is shown in Fig. 1 as blue dashed line, which has a deviation of 11.9° between the *ab initio* direction (*vide post*).

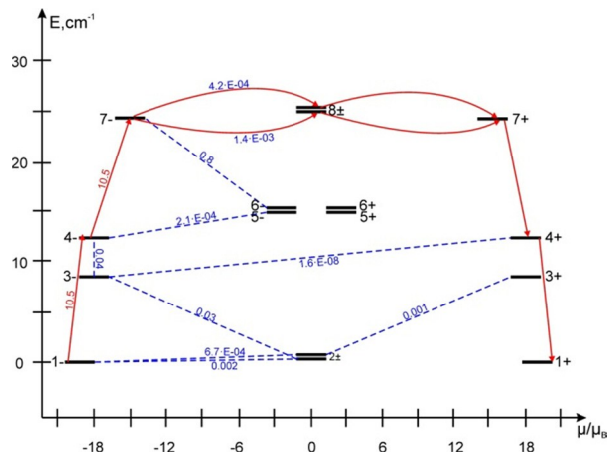


Fig. 5 Low-lying exchange spectrum in **1-RR**. The two states of each exchange doublet $n\pm$ are placed according to the value of the projection of their magnetic moment on the main magnetic axis of the ground exchange doublet (bold black lines). Vertical dashed lines show the spin-phonon transitions, with the numbers showing averaged transition moments (in μ_B) between the corresponding states. The red arrows outline the relaxation path of magnetization.

The above experimental results were further confirmed and rationalized by the *ab initio* calculations performed on the complete molecular structure of **1-RR** (Fig. S21, see ESI for details[†]).^{8b, 21} As can be seen in Table S7, the calculated ground doublets of the Tb^{3+} ions are both well separated from the first excited states located at the energy of 200 cm^{-1} higher. The Ising anisotropy of the ground doublets was confirmed by the very large g_z values (17.90, Table S8) of the ground doublets. Furthermore, the calculated easy axes of the individual Tb^{3+} centers were almost parallel to each other (Fig. 1), in consistent with the presence of the pseudo-inversion center. The magnetic interactions in **1-RR** were simulated with a pseudospin exchange Hamiltonian (Eq. S1).^{5c, 8b} Simultaneous simulation of $\chi_M T$ - T and M - H curves (Fig. S4-5) provides the following coupling parameters: $J_{\text{Cu-Tb}} = 25.3 \text{ cm}^{-1}$, $J_{\text{Tb-Tb}} = 4.3 \text{ cm}^{-1}$, $J_{\text{Cu-Cu}} = -3.2 \text{ cm}^{-1}$, entering the effective Ising Hamiltonian for the low-lying multiplets (Eq. S2, Table S9). With these exchange parameters obtained, the exchange spectrum of the cluster were calculated and shown in Table S10. As we can see, the resulting exchange spectrum shows negligible tunnelling splitting for all exchange doublets, thus outlining a barrier of blocking of magnetization of ca. 25 cm^{-1} , which is in good agreement with the experimental value. This is further confirmed by construction of the blocking barrier of magnetization following a recently proposed methodology.²⁵ The relaxation path of magnetization was found by connecting the exchange states with the largest transition moments (Fig. 5). It contains intense spin-phonon-transitions $1\pm \leftrightarrow 4\pm$ and $4\pm \leftrightarrow 7\pm$, and a temperature-assisted QTM $7- \leftrightarrow 8\pm \leftrightarrow 7+$ which becomes possible in the presence of internal

magnetic fields bringing in resonance the states 7 and 8. This analysis shows that the observed blocking barrier is of the exchange origin.

Moreover, due to relatively strong ferromagnetic exchange interaction between the terbium and (isotropic) copper centres, the local magnetic moments of Cu^{2+} in the ground exchange doublet are aligned along the main magnetic axes of terbium (Fig. 1). These results allow concluding that the extracted anisotropy axis of the complex coincides with the calculated anisotropy axes on the two Tb sites. The angular dependence of the magnetic susceptibility of **1-RR** at 3 K was also calculated *ab initio* and depicted in Fig. 4 by dashed lines. For the curves rotating around y axis, the match of the experiment and calculated curves is very good with a small difference of the absolute values, which is reasonable considering the small magnetic field of the single crystal. For the curves rotating along the x and z directions, the offset is about 10° , reflecting the deviation between the measured and calculated directions.

For the magnetostructural relationship, the main anisotropy axis of the Tb^{3+} ion is directed approximately perpendicular to the triangles of the bicapped trigonal prism, as in the case of other sandwiched complexes.^{24, 23} Furthermore, we can see that in the coordination geometry of the Tb^{3+} ion, there is a pseudo-mirror plane formed by atoms Tb1, N11 and N14 (Fig. S22). According to the Neumann's principle,²⁴ the easy axis of Tb^{3+} should be related to a symmetry operation, i.e., lie within the mirror plane, as confirmed by experimental and *ab initio* analysis. These conclusions were also reproduced by a simple electrostatic crystal field calculation involving point charges on coordination atoms taken as Mulliken charges obtained from DFT calculations (see ESI).^{7c-d} The direction of the main anisotropy axis in these calculations coincides with the direction of the lowest energy in the electrostatic potential energy surface (Fig. S22). However, the deviation of this axis from the measured one amounts to 20.8° , twice larger than for the *ab initio* calculated anisotropy axis. This shows the limitation of the electrostatic model that does not take into account the metal-ligand covalency effects in the crystal field of lanthanide, which are treated in angular-overlap model (AOM).^{6b, c} The latter models are expected to give results of similar accuracy for the direction of the main anisotropy axis, which thus is basically determined by the geometry of the surrounding ligand atoms rather than exclusively by their electrostatic charges. Comparison of *ab initio* with simplified electrostatic crystal field calculations show that all contributions to the ligand field have to be taken into account in order to obtain a deeper understanding of the magnetic anisotropy of the Ln complexes.

Conclusions

In summary, two enantiomeric tetranuclear $[\text{CuTb}]_2$ SMMs were characterized and their magneto-structural relationship was carefully studied. Angular resolved magnetometry measurements and *ab initio* calculations were performed on a multinuclear SMM for the first time, to establish the Ising magnetic anisotropy of both the whole molecule and the Tb^{3+} centers. Further studies on the isostructural compounds with other 3d-4f combinations ($[\text{CuLn}]_2$, $[\text{ZnLn}]_2$ etc.) are in progress to systematically investigate their magneto-structural relationships, in the hope of enlightening the rational design of better performing SMMs.

This work is supported by the "973 project" (2013CB922102), NSFC (91022031, 21101093, 21471077). This work was also supported by a Project Funded by the Priority Academic Program Development of Jiangsu Higher Education Institutions. VV and LFC acknowledge the support of the Flemish Science Foundation (FWO) and of the University of Leuven through the INPAC and Methusalem programs.

Notes and references

^a State Key Laboratory of Coordination Chemistry, Collaborative Innovation Center of Advanced Microstructures, School of Chemistry and Chemical Engineering, Nanjing University, Nanjing, 210093, China. E-mail: wangxy66@nju.edu.cn.

^b Theory of Nanomaterials Group and INPAC - Institute of Nanoscale Physics and Chemistry, Katholieke Universiteit Leuven, Celestijnenlaan 200F, 3001 Heverlee, Belgium. E-mail: liviu.Chibotaru@chem.kuleuven.be.

^c Institut Néel, CNRS & UJF BP 166, 38042, Grenoble Cedex 9, France.

^d LNCMI-CNRS 25, rue des Martyrs-BP 166, 38042, Grenoble Cedex 9, France. E-mail: jiang@lncmi.cnrs.fr.

[†] Electronic Supplementary Information (ESI) available: experimental section, solid-state circular dichroism (CD) spectra, X-ray crystallography data, additional magnetic measurements and theoretical calculations. See DOI: 10.1039/b000000x/

1 J. M. D. Coey, *Magnetism and Magnetic Materials*, Cambridge University Press, 2010.

2 (a) O. Waldmann, *Inorg. Chem.*, 2007, **46**, 10035; (b) F. Neese and D. A. Pantazis, *Faraday Discuss.*, 2011, **148**, 229.

3 L. Bogani and W. Wernsdorfer, *Nature Mater.*, 2008, **7**, 179.

4 (a) M. N. Leuenberger and D. Loss, *Nature*, 2001, **410**, 789; (b) F. Troiani and M. Affronte, *Chem. Soc. Rev.*, 2011, **40**, 3119.

5 (a) D. N. Woodruff, R. E. P. Winpenny and R. A. Layfield, *Chem. Rev.*, 2013, **113**, 5110; (b) F. Habib and M. Murugesu, *Chem. Soc. Rev.*, 2013, **42**, 3278; (c) R. J. Blagg, L. Ungur, F. Tuna, J. Speak, P. Comar, D. Collison, W. Wernsdorfer, E. J. L. McInnes, L. F. Chibotaru and R. E. P. Winpenny, *Nat. Chem.*, 2013, **5**, 673;

6 (a) A. Abragam and B. Bleaney, *Electron Paramagnetic Resonance of Transition Ions*, Clarendon, Oxford, 1970; (b) C. K. Jørgensen, *Adv. Chem. Phys.*, 1963, **5**, 33; (c) B. N. Figgis and M. A. Hitchman, *Ligand Field Theory and Its Applications*, Wiley-VCH, New York, 1999.

7 (a) J. J. Baldoví, J. J. Borrás-Almenar, J. M. Clemente-Juan, E. Coronado and A. Gaita-Ariño, *Dalton Trans.*, 2012, **41**, 13705; (b) J. J. Baldoví, S. Cardona-Serra, J. M. Clemente-Juan, E. Coronado, A. Gaita-Ariño and A. Palli, *J. Comput. Chem.*, 2013, **34**, 1961; (c) N. F. Chilton, D. Collison, E. J. L. McInnes, R. E. P. Winpenny and A. Soncini, *Nat. Commun.*, 2013, **4**, 2551; (d) V. S. Mironov, Y. G. Galyametdinov, A. Ceulemans and K. Binnemans, *J. Chem. Phys.*, 2000, **113**, 10293.

8 (a) L. F. Chibotaru and L. Ungur, *J. Chem. Phys.*, 2012, **137**, 064112; (b) L. F. Chibotaru, L. Ungur and A. Soncini, *Angew. Chem. Int. Ed.* 2008, **47**, 4126; (c) L. Ungur and L. F. Chibotaru, *Phys. Chem. Chem. Phys.*, 2011, **13**, 20086; (d) K. Bernot, J. Luzon, L. Bogani, M. Etienne, C. Sangregorio, M. Shanmugam, A. Caneschi, R. Sessoli and D. Gatteschi, *J. Am. Chem. Soc.*, 2009, **131**, 5573.

9 (a) J. Z. Sievers, *Phys. B Con. Mat.*, 1982, **45**, 289; (b) J. D. Rinehart and J. R. Long, *Chem. Sci.*, 2011, **2**, 2078; (c) A. Yamashita, A. Watanabe, S. Akine, T. Nabeshima, M. Nakano, T. Tamamura and T. Kajiwara, *Angew. Chem. Int. Ed.*, 2011, **50**, 4016.

10 (a) M. Gerloch and D. J. Mackey, *J. Chem. Soc. A* 1971, 3372 and references therein; (b) S. Mitra, *Trans. Metal Chem.* 1972, **7**, 183; (c) S. Mitra, *Prog. Inorg. Chem.* 1977, **22**, 309.

11 (a) G. Cucinotta, M. Perfetti, J. Luzon, M. Etienne, P. E. Car, A. Caneschi, G. Calvez, K. Bernot and R. Sessoli, *Angew. Chem. Int. Ed.* 2012, **51**, 1606; (b) M. E. Boulon, G. Cucinotta, J. Luzon, C. Degl'Innocenti, M. Perfetti, K. Bernot, G. Calvez, A. Caneschi and R. Sessoli, *Angew. Chem. Int. Ed.*, 2013, **52**, 350; (c) T. T. da Cunha, J. Jung, M. E. Boulon, G. Campo, F. Pointillart, C. L. M. Pereira, B. Le Guennic, O. Cador, K. Bernot, F. Pineider, S. Golhen and L. Ouahab, *J. Am. Chem. Soc.*, 2013, **135**, 16332; (d) J. Jung, F. Le Natur, O. Cador, F. Pointillart, G. Calvez, C. Daiguebonne, O. Guillou, T. Guizouarn, B. Le Guennic, K. Bernot, *Chem. Commun.*, 2014, **50**, 13346.

12 (a) M. E. Boulon, G. Cucinotta, S. S. Liu, S. D. Jiang, L. Ungur, L. F. Chibotaru, S. Gao and R. Sessoli, *Chem. Eur. J.*, 2013, **19**, 13726; (b) M. Perfetti, G. Cucinotta, M. E. Boulon, F. E. Hallak, S. Gao and R. Sessoli, *Chem. Eur. J.*, 2014, **20**, 14051.

13 J. Jung, T. T. da Cunha, B. Le Guennic, F. Pointillart, C. L. M. Pereira, J. Luzon, S. Golhen, O. Cador, O. Maury and L. Ouahab, *Eur. J. Inorg. Chem.*, 2014, 3888.

14 N. Ishikawa, M. Sugita, T. Ishikawa, S. Koshihara and Y. Kaizuka, *J. Am. Chem. Soc.*, 2003, **125**, 8694.

15 S. Osa, T. Kido, N. Matsumoto, N. Re, A. Pochaba and J. Mroziński, *J. Am. Chem. Soc.*, 2004, **126**, 420.

16 C. R. Ganivet, B. Ballesteros, G. de la Torre, J. M. Clemente-Juan, E. Coronado and T. Torres, *Chem. Eur. J.*, 2013, **19**, 1457.

17 J. D. Rinehart, M. W. Fang, J. Evans and J. R. Long, *J. Am. Chem. Soc.*, 2011, **133**, 14236.

18 X. C. Huang, C. Zhou, H. Y. Wei and X. Y. Wang, *Inorg. Chem.*, 2013, **52**, 7314.

19 (a) J. P. Costes, F. Dahan and W. Wernsdorfer, *Inorg. Chem.*, 2006, **45**, 5; (b) J. P. Costes, M. Auchel, F. Dahan, V. Peyrou, S. Shova and W. Wernsdorfer, *Inorg. Chem.*, 2006, **45**, 1924.

20 K. S. Cole and R. H. Cole, *J. Chem. Phys.*, 1941, **9**, 341.

21 F. Aquilante, L. DeVico, N. Ferre, G. Ghigo, P. A. Malmqvist, P. Neogrady, T. B. Pedersen, M. Pitonak, M. Reiher, B. O. Roos, S. J. A. Andres, M. Urban, V. Veryazov, R. Lindh, *J. Comput. Chem.*, 2010, **31**, 224.

22 (a) W. Wernsdorfer, N. Aliga-Alcalde, D. N. Hendrickson and G. Christou, *Nature*, 2002, **416**, 406; (b) S. Hill, R. S. Edwards, N. Aliga-Alcalde and G. Christou, *Science*, 2003, **302**, 1015.

23 (a) L. Ungur, J. J. Le Roy, I. Korobkov, M. Murugesu and L. F. Chibotaru, *Angew. Chem. Int. Ed.*, 2014, **53**, 4413; (b) R. Marx, F. Morlock, M. Dörfel, L. Ungur, M. Waters, S. D. Jiang, M. Orlita, J. Taylor, W. Frey, L. F. Chibotaru and J. van Slageren, *Chem. Sci.*, 2014, **5**, 3287.

24 A. Authier, Eds. *International Tables for Crystallography, Volume D: Physical Properties of Crystals*, Kluwer Academic Publisher, 2001, section I.1.4.

25 L. Ungur, M. Thewissen, J. P. Costes, W. Wernsdorfer, L. F. Chibotaru, *Inorg. Chem.*, 2013, **52**, 6328.